Supporting Information

I-motif Formed at Physiological pH Triggered by Spatial Confinement of Nanochannels: An Electrochemical Platform for pH Monitoring in Brain Microdialysates

Lu Shi, Feifei Cao, Limin Zhang*, and Yang Tian

School of Chemistry and Molecular Engineering, East China Normal University, Dongchuan Road 500, Shanghai 200241, China.

Contents

1. Experimental section

In Vivo Microdialysis. All procedures involving animals were conducted with approval of the Animal Ethics Committee in East China Normal University, China. Surgeries for in vivo microdialysis were performed as reported previously.[S1] Briefly, adult male Sprague-Dawley normal rats and ischemia model rats (200-250 g, Shanghai SLAC Laboratory animal Co. Ltd., China) were anaesthetized with chloral hydrate (initial dose of 300 mg/kg, (i.p.) with additional doses of 50 mg/kg (i.p.) as needed to maintain anesthesia) and positioned onto a stereotaxic frame (Beijing Tide-Gene Biotechnology Development Centre). The microdialysis probe (CMA/110/111 Tub) was implanted in the striatum at the site of 2.5 mm anterior to bregma, 2.5 mm lateral from midline, and 7.0 mm below dura. In order to reduce injury to the rat, the microdialysis probe should be implanted into the striatum of rats slowly within 30 min with special care. Throughout the surgery, the body temperature of the animals was maintained at 37°C with a home-made thermic blanket (Beijing Tide-Gene Biotechnology Development Centre). The microdialysis probes (CMA/110/111 Tub) were implanted into the striatum of rats and were perfused with an aCSF solution at 2 μL min^{-1} for at least 90 min for equilibration.

Molecular dynamics simulations

All the all-atom MD simulations were based on a general AMBER force field with the RESP charges and were carried out using the Gromacs-4.6.7 software package.[S2-S4] The system is a relaxed liquid configuration at 298K and 1 bar. A 2 ns NVT relaxation run and a 2 ns NPT relaxation run were performed before production simulation. The time step was 1 fs, and the total run time was 10 ns for the equilibrium MD simulation. We used the relaxed system as a starting configuration. As it is prior to system relaxation MD, energy minimization was carried out with a composite protocol of steepest descent using termination gradients of 100 KJ/mol•nm. The Nose´-Hoover thermostat[S5] was used to maintain the equilibrium temperature at 298 K and periodic boundary conditions were imposed on all three dimensions. The Particle Mesh-Ewald method [S6, S7] was used to compute long-range electrostatics within a relative tolerance of $1x10^{-6}$. A cut-off distance of 1nm was applied to real-space Ewald interactions. The same value was used for van der Waals interactions. The LINCS algorithm[S8] was applied to constrain bond lengths of hydrogen atoms. A

leap-frog algorithm[S9] was used with a time step of 1 fs.

References:

[S1] Shao, X.; Gu, H.; Wang, Z.; Chai, X.; Tian, Y.; Shi, G. *Anal. Chem.,* **2013,** *85,* 418.

[S2] Wang, J.; Wolf, R. M.; Caldwell, J. W.; Kollman, P. A.; Case, D. A. *J. Comput. Chem.,* **2004,** *25,* 1157.

[S3] Bayly, C. I.; Cieplak, P.; Cornell, W.; Kollman, P. A. *J. Phys. Chem.,* **1993,** *97,* 10269.

[S4] Hess, B.; Kutzner, C.; Spoel, D.; Lindahl, E. *J. Chem. Theory Comput.,* **2008,** *4,* 435.

[S5] Berendsen, H. J.; Postma, J. P. M.; Van Gunsteren, W. F.; DiNola, A.; Haak, J. *J. Chem. Phys.* **1984,** *81,* 3684.

[S6] Essmann, U.; Perera, L.; Berkowitz, M. L.; Darden, T.; Lee, H.; Pedersen, L. G. *J. Chem. Phys.* **1995,** *103,* 8577.

[S7] Astrakas, L. G.; Gousias, C.; Tzaphlidou, M. *J. Appl. Phys.* **2012,** *111,* 074702.

[S8] Hess, B.; Bekker, H.; Berendsen, H. J.; Fraaije, J. G. *J. Comput. Chem.* **1997,** *18,* 1463.

[S9] Van Gunsteren, W. F.; Berendsen, H. *Mol. Simul.* **1988,** *1,* 173.

2. CV characterization of the modification step of ITO/SC/DNA-1.

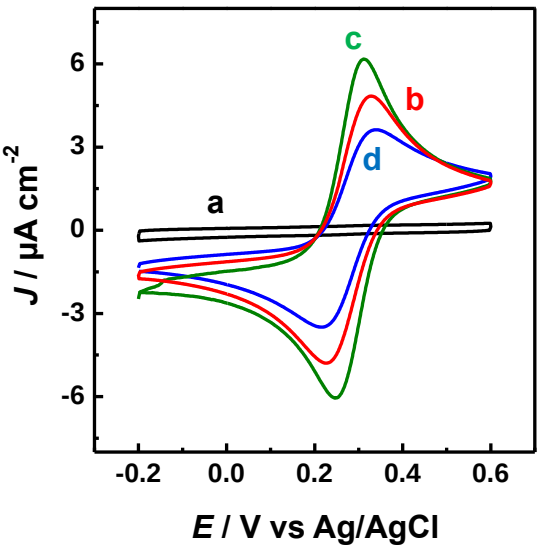

Figure S1. CVs of silica nanochannel-modified ITO electrode (a) before and (b) after removal of CTAB microcells, (c) ITO/SC/APTS, and (d) ITO/SC/DNA-1 electrode in phosphate buffer containing 0.1 M NaCl and 50 μM $[Fe(CN)_6]^{3-}$.

3. Stability of anodic peak current.

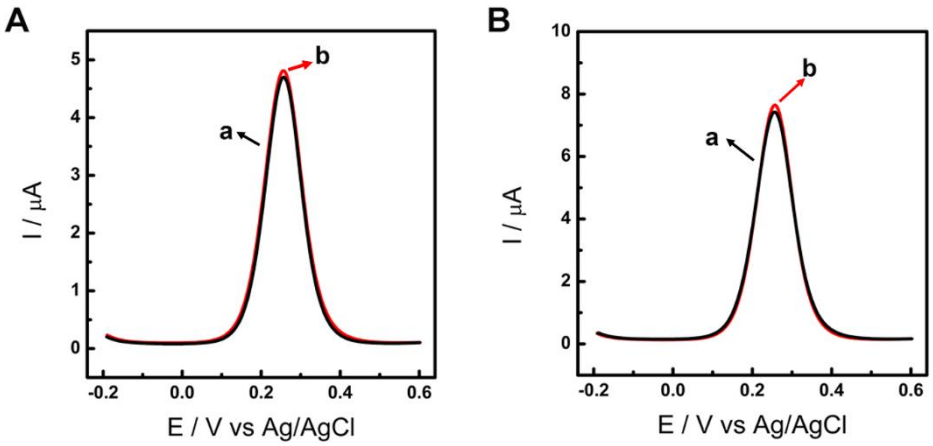

Figure S2. DPV curves recorded at the ITO/SC/DNA-3 in phosphate buffer containing 0.1 M NaCl and 50 μM $[Fe(CN)_6]^{3-}$ under pH 5.5 (A) and pH 7.4 (B) before (curve b) and after continuous scanning for 50 cycles (curve a), respectively.

4. DPVs obtained at ITO/SC/APTS electrode.

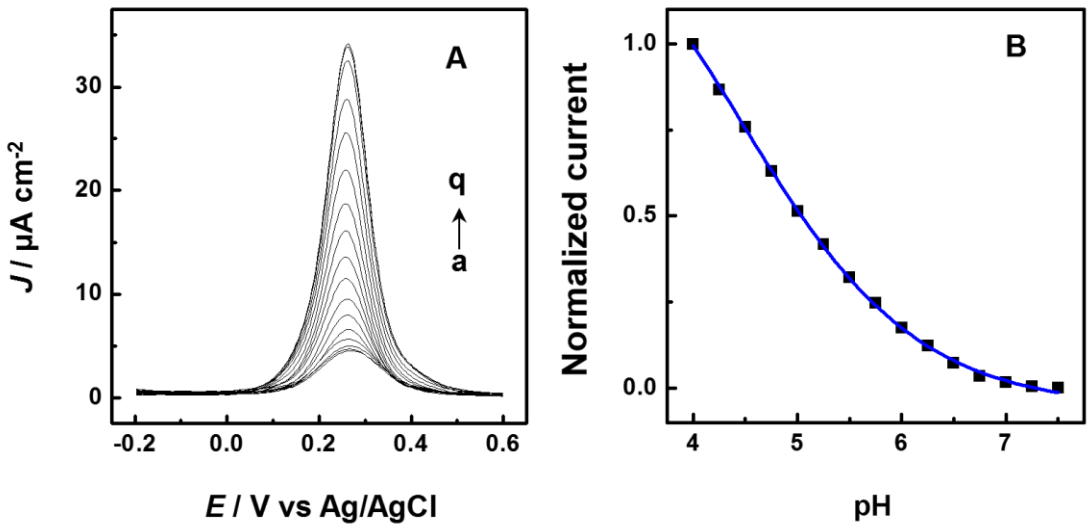

Figure S3. (A) DPVs obtained at ITO/SC/APTS in phosphate buffer containing 0.1 M NaCl and 50 μM $[Fe(CN)_6]^{3-}$ under different pH, which are (a) 8.00，(b) 7 .50，(c) 7.25，(d) 7.00，(e) 6.75，(f) 6.50，(g) 6.25，(h) 6.00，(i) 5.75，(j) 5.50，(k) 5.25，(l) 5.00，(m) 4.75, (n) 4.50，(o) 4.25，(p) 4.00，(q) 3.75, respectively. (B) Plot of the normalized current versus pH values.

5. Response time.

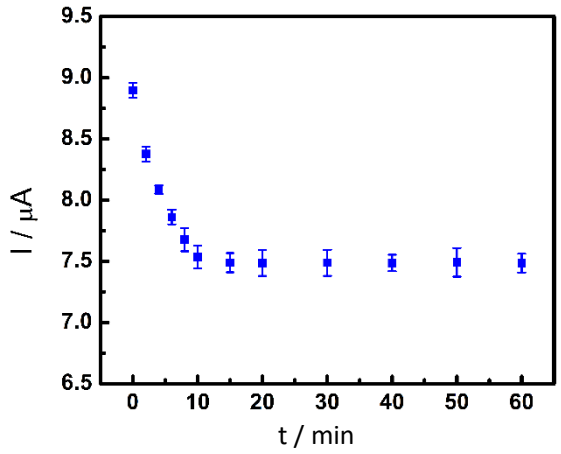

Figure S4. The relationship between anodic peak current and time obtained at ITO/SC/DNA-3 in phosphate buffer containing 0.1 M NaCl and 50 μM $[Fe(CN)_6]^{3-}$ under pH 7.4.

6. pH dependent CD spectra in diluted solution.

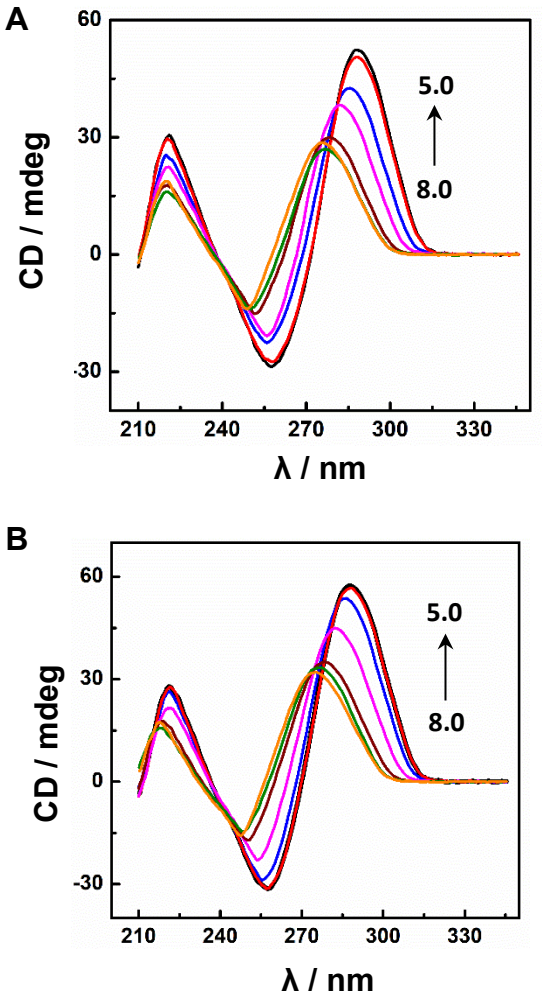

Figure S5. CD spectra of (A) DNA-1, (B) DNA-2 in phosphate buffer containing 0.1 M NaCl with different pH.

7. Plot of normalized current vs pH at ITO/DNA-3 electrode.

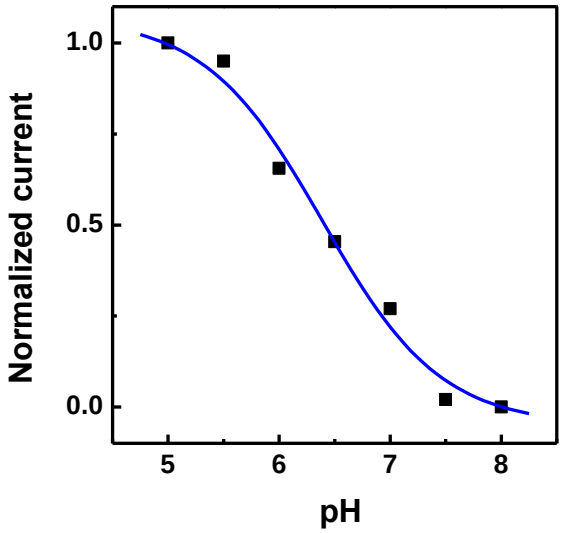

Figure S6. Plot of the normalized current obtained at ITO/DNA-3 in phosphate buffer containing 0.1 M NaCl and 50 μM $[Fe(CN)_6]^{3-}$ vs pH values.

8. XPS with the depth analysis

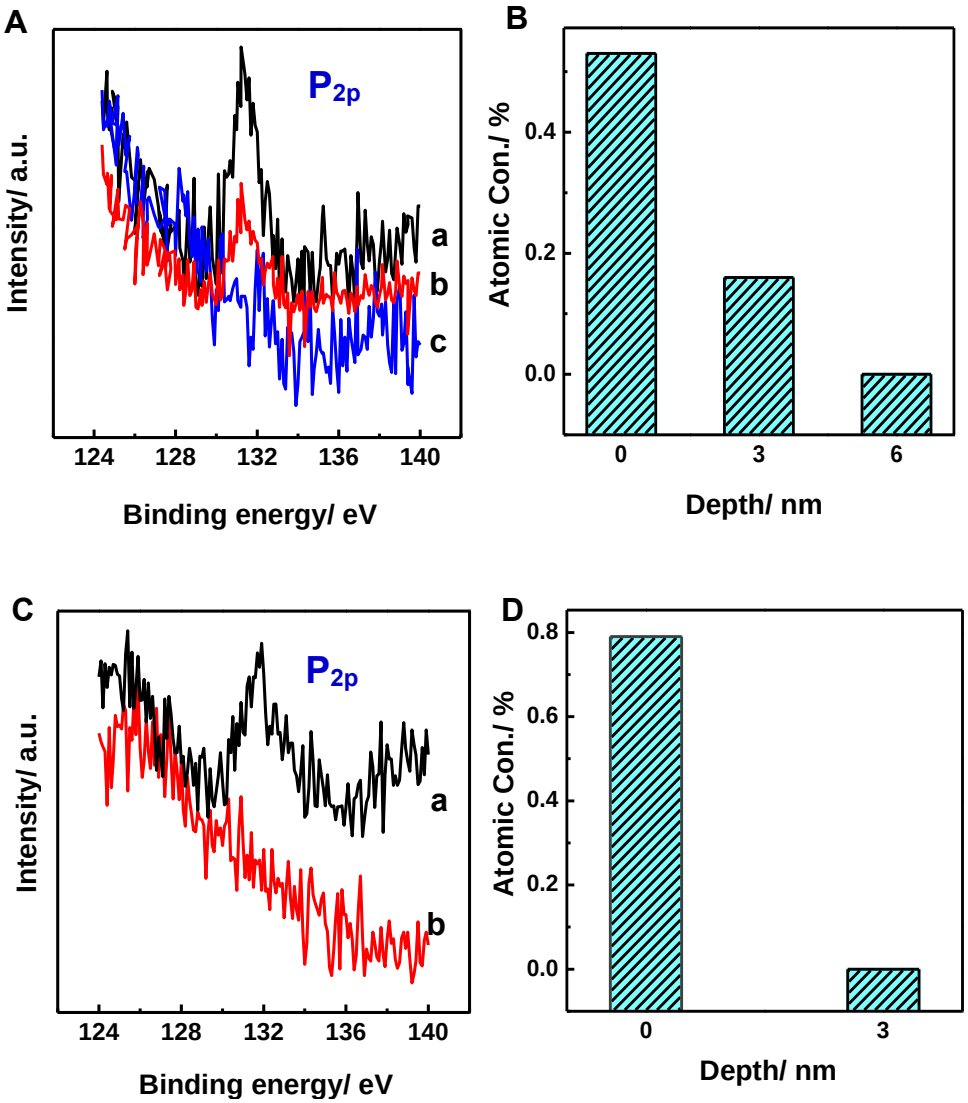

Figure S7. (A, C) P_{2P} spectra with depth of (a) 0 nm, (b) 3 nm, and (c) 6 nm, and (B, D) their corresponding P_{2p} atomic concentration under different depth for (A, B) ITO/SC/DNA-3 and (C, D) ITO/SC/DNA-3' electrode.

9. Plots of normalized current vs pH at ITO/SC/DNA-n' electrodes.

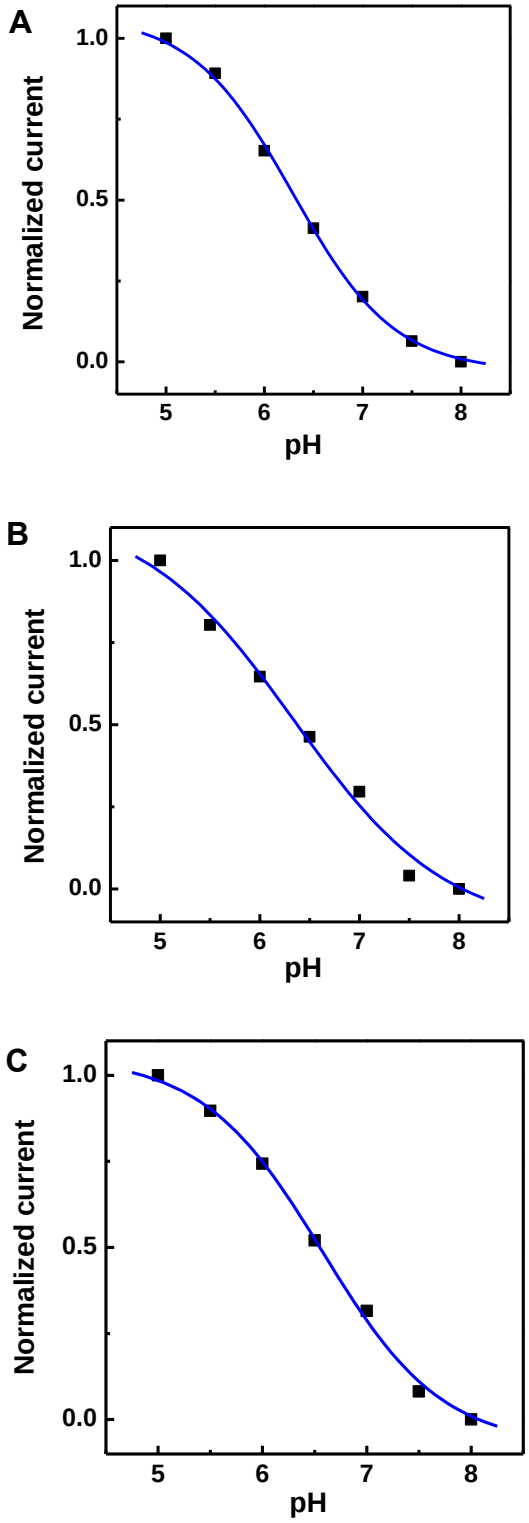

Figure S8. Plots of normalized current vs pH at (A) ITO/SC/DNA-1', (B) ITO/SC/DNA-2', and (C) ITO/SC/DNA-3' electrodes.

10. Schematic illustration of mass transport at ITO/SC/DNA-n'

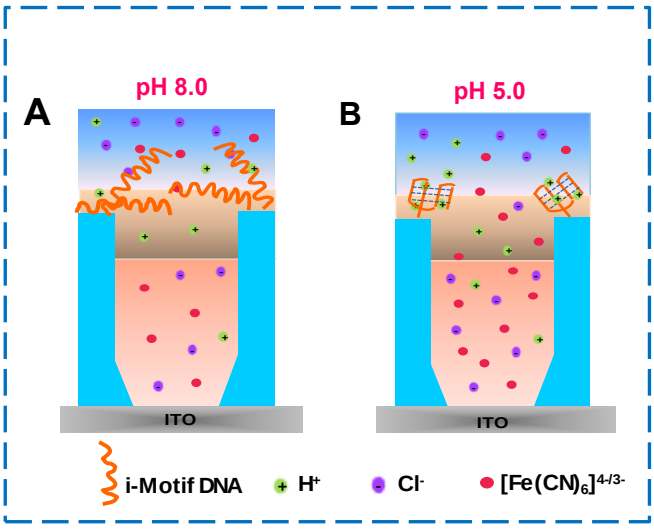

Figure S9. Schematic illustration of mass transport at ITO/SC/DNA-n' electrode under different pH values.

11. Plot of normalized current vs pH at low ionic strength

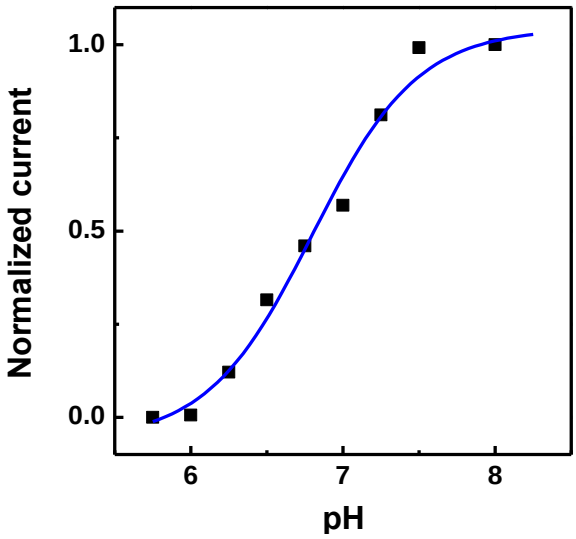

Figure S10. The plot of normalized current versus pH value obtained at the ITO/SC/DNA-3 electrode in phosphate buffer containing 10 mM NaCl and 50 μM $[Fe(CN)_6]^{3-}$.

12. Plots of normalized current vs pH in nanochannels with different pores.

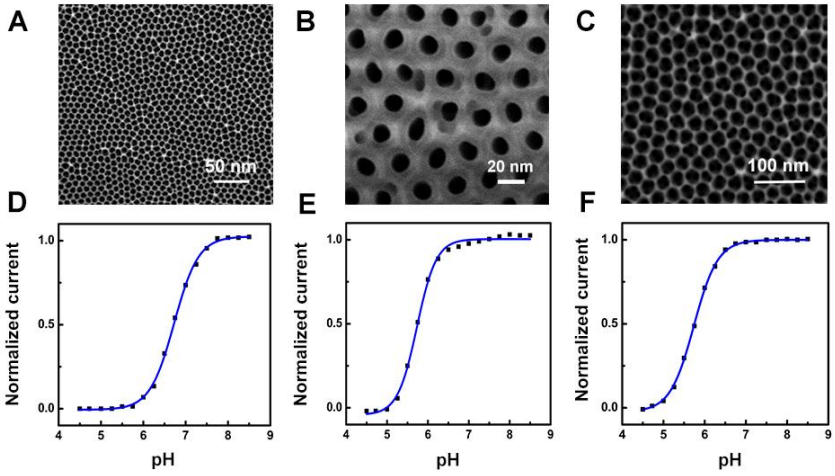

Figure S11. (A-C) The top-view TEM images of nanochannels with (A) 10 nm, (B) 20 nm, and (C) 30 nm pores. (D-F) The plots of normalized current vs pH in nanochannels with (D) 10 nm, (E) 20 nm, and (F) 30 nm pores.

13. DFT calculation.

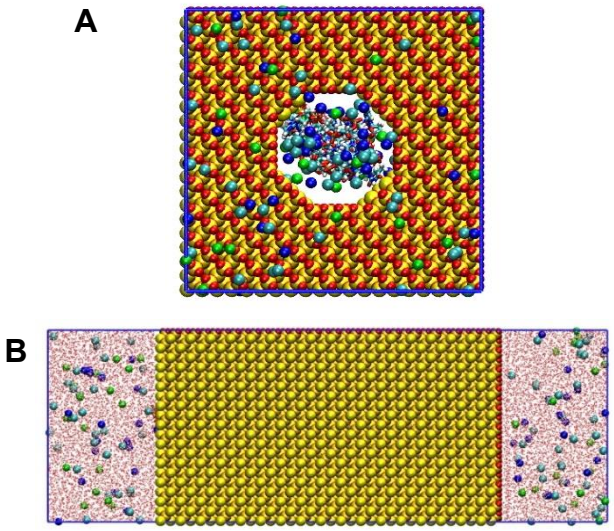

Figure 12. (A) The front view and (B) lateral view of single silica nanochannel modified by DNA-3 in 0.1 M NaCl.

14. Selectivity test

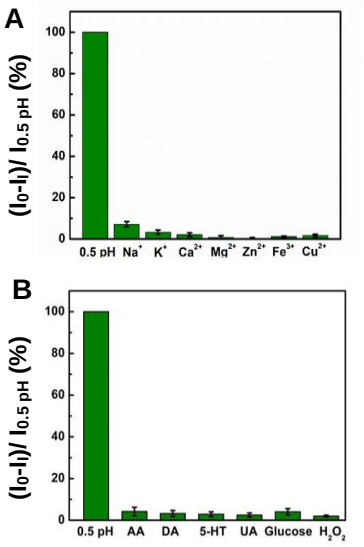

Figure S13. Selectivity test for pH obtained at ITO/SC/DNA-3 in the presence of (A) various metal ions: K^+, Na^+, Ca^{2+}, Mg^{2+}, Zn^{2+}, Fe^{3+}, and Cu^{2+} (150 mM for Na^+, 3 mM for K^+, 1 mM Ca^{2+} and Mg^{2+}, 10 μM for others metal ions), and (B) potential interfering compounds in rat brain. Their concentrations are 200 μM AA, 50 nM DA, 50 nM 5-HT, 20 μM UA, 5 mM Glucose, and 500 nM H_2O_2, respectively. The Error bars indicate standard deviations (n=3, S.D.).

15. Reversibility test

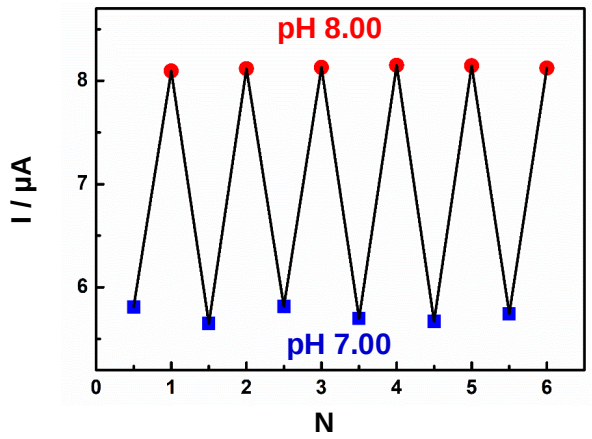

Figure S14. Reversibility of ITO/SC/DNA-3 in phosphate buffer containing 0.1 M NaCl and 50 µM $[Fe(CN)_6]^{3-}$ under pH 8.0, and 7.0.